Desalination and Water Treatment
www.deswater.com

doi: 10.5004/dwt.2021.27437

230 (2021) 419–429
August

UV degradation of naproxen adsorbed on graphite oxide

Adem Sarihan[a], Senay Balbay[b,*]

[a]*Department of Chemical Technology, Bilecik Seyh Edebali University, Vocational School, 11230 Bilecik, Turkey, email: adem.sarihan@bilecik.edu.tr*
[b]*Department of Waste Management, Bilecik Seyh Edebali University, Vocational School, 11230 Bilecik, Turkey, email: senay.balbay@bilecik.edu.tr*

Received 2 March 2021; Accepted 15 May 2021

ABSTRACT

In the study, it was aimed to remove naproxen sodium (NPX) adsorbed on graphite oxide produced from commercial graphite by degrading it under UV effect. Temperature (25°C–50°C), adsorbent amount (1–3 g/50 mL), pH (3–9), contact time (15–1440 min) and initial concentration (20–150 ppm) were selected as parameters. The scanning electron microscopy morphological images, X-ray diffraction mineralogical content, Fourier-transform infrared spectroscopy functional group analysis, Brunauer–Emmett–Teller surface areas of adsorbents were determined. It was observed that the NPX removal efficiency of graphite (11.56%) was much lower (73.29%) than graphite oxide (GRO). Determination of the desorption% of UV degradation studies of adsorbed GRO's at the end of 1, 2 and 3 h as 47.5%, 34.06% and 31.59% respectively, proved that the UV degradation is effective in the removal of NPX attached to the GRO surface. As a result, it was observed that UV degradation was effective in removing NPX from the GRO surface.

Keywords: Naproxen; Graphite oxide; Commercial graphite; UV degradation

1. Introduction

Increasing global drug production and high drug consumption cause natural water resources, drinking water and wastewater to be contaminated by pharmaceutical components, which is seen as an important environmental problem [1,2]. Among the pharmaceutical components "nonsteroidal anti-inflammatory" drugs (with pain-relieving and antipyretic effects) are the most widely used drug group with the highest risk of causing environmental pollution [2]. Naproxen sodium ($C_{14}H_{13}NaO_3$) is one of the most commonly used drug active substances in this drug group (Fig. 1) [3,4]. Due to its biological activity, naproxen sodium has the risk of adversely affecting living organisms and reducing biodiversity in the natural environment [5]. As a result of studies conducted on aquatic organisms, it was determined that naproxen sodium adversely affected the gastrointestinal system and kidneys of aquatic organisms [6], doses above 115.2 and 147.6 ppm for embryos and larvae, respectively, were fatal and damaged liver tissues [7]. In addition, as a result of studies conducted on mice, it was observed that this drug has the potential to cause genotoxicity [8]. Therefore, naproxen sodium is considered to be a potential threat especially for aquatic organisms and an important environmental pollutant. Thus, removing naproxen sodium from aqueous environments is seen as an important field of study. Various techniques such as membrane [9], ion exchange [10], biodegradation [11], catalytic oxidation [12] and ozonation [13] have been given in the literature for the removal of naproxen sodium from aqueous media. Compared to these methods, adsorption is an important alternative technique with

* Corresponding author.

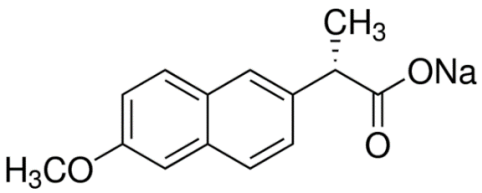

Fig. 1. Chemical structure of naproxen sodium.

advantages such as being more economical, simple to apply and highly effective removal potential [5].

Graphite oxide (GRO) is a popular and potential two-dimensional nanomaterial with many advantages including dispersibility and affinity for many contaminants in water, low density and high adsorption capacity [14]. It has attracted great attention in recent years due to its unique properties such as hydrophilic property, presence of functional groups, graphene alternative, and a flat form of various composites for different applications [15]. Graphite oxide is one of the most important precursors of graphene and has a layered structure consisting of layer structures similar to graphene due to its properties such as high adsorption capacity and stability [16,17]. It is an effective adsorbent in which polar and certain non-polar solvents can be placed in the interlayer space. GRO adsorbs polar adsorbents more easily than non-polar adsorbents due to certain interactions with polar groups on it [18]. During the oxidation process, these layers were wrinkled due to the change in hybridization of carbon atoms with the simultaneous addition of oxygen-containing functions (hydroxyls, epoxides, ketones, carboxyls, etc.). GRO consists of layers of sp2-hybridized carbon atoms containing covalently bonded oxygen functions that can be placed at the edges or basal planes of carbon layers. Carboxyl functionalities are generally found at the edges of individual layers. There are other oxygen functions such as hydroxyls, epoxides and ethers on the surface of the layers [19,20]. Interest in GRO has resurfaced over the past decade due to the fact that graphene-based materials are cost-effective and scalable and play a leading role in their preparation [20]. Compared to pure graphite, GRO's interlayer distance increases significantly from 3.4 Å to 6–12 Å depending on the oxidation procedure. The presence of water molecules added to the interlayer space is obvious and cannot be ignored when defining GRO. Since graphite is a very inert mineral, it can be oxidized by very strong oxidizing agents. The structure of the prepared GRO is strongly affected by the starting material used, the oxidation process and even the purification process [19].

Researchers produced graphene oxide nanopowder modified with the Hummer method and obtained a maximum removal efficiency of naproxen sodium (NPX) of 65.28% under optimum conditions [21]. 86% NPX removal efficiency was obtained by using amine-functionalized reduced graphene oxide [22]. A maximum of 190 mg/g of humic acid adsorption was achieved on graphite oxide produced from graphite. This outcome is higher than the adsorption of humic acid on activated carbon and graphite [17]. NPXs, which are very permanent against biological degradation, can stay in the aquatic environment for a long time due to their high hydrophilicity and stability in water. They have often been observed in wastewater, surface water and groundwater, due to their release into the water through various routes, such as urinary and improper disposal [23]. The detection of NPX (as a contaminant) up to 2.3 mg/L in wastewater effluent worldwide highlights the fact that NPX (and many other Petroleum Hydrocarbons) often cannot be effectively removed by conventional wastewater treatment. NPX is currently on the Global Water Research Coalition (GWRC) priority list [24]. Determination of trace level concentrations of this drug in water bodies as water pollution due to the presence of NPX in almost all water samples such as rivers, wells and wastewater is of great interest [25].

Many studies have been conducted on the removal of NPX, which is such an important compound, by the adsorption method. Little research has been reported on GRO's adsorption applications [17]. There are no studies in the literature regarding the removal of NPX by using GRO and the reusability of adsorbed GRO by cleaning under UV effect. The degradation of naproxen adsorbed on graphite oxide produced from commercial graphite under UV effect is the subject of this study and the study will contribute to the literature in this respect.

2. Material and method

2.1. Material

Commercial graphite (in powder form) (GR) was obtained from SKC Karbon. Potassium permanganate ($KMnO_4$), HCl, hydrogen peroxide (H_2O_2), NaOH, sodium nitrate ($NaNO_3$) and sulfuric acid (H_2SO_4) chemicals were purchased from Merck (Germany). Naproxen sodium (NPX) was supplied from Sigma (Germany). NaOH and HCl chemicals were used for pH studies. Analytical grade chemicals are used.

2.2. Graphite oxide production

Graphite oxide was produced using graphite according to Hummers Method [26]. Firstly, 5 g graphite powder, 2.5 g sodium nitrate ($NaNO_3$), 115 mL 96% sulfuric acid (H_2SO_4) were mixed in a beaker and continued to be stirred in an ice bath for 1 h. Keeping the bath temperature below 5°C, 15 g of potassium permanganate ($KMnO_4$) was slowly added to the mixture. After obtaining a homogeneous mixture, it was mixed for 2 h at 35°C–40°C temperature range. Secondly, 500 mL of deionized water was slowly added to the mixture and stirred for 1 h. 8.4 mL of hydrogen peroxide (35.7%) was added to the mixture so that the temperature was <40°C, and it was stirred for a further 2 h. Thirdly, GRO produced was filtered and washed to pH 7 with distilled water.

2.3. Batch experiments

The NPX standard stock solution was prepared using purified water at a concentration of 1,000 ppm. This solution is diluted for the desired concentrations. NPX adsorption kinetics and isotherms were obtained under different

operating conditions using batch reactors. Adsorption kinetics was studied for different pH (3, 5, 6, 7, 9), contact time (15, 30, 60, 120, 180, 300, and 1,440 min) and adsorbent amount (1, 2, 3 g/50 mL) at 50 ppm of initial NPX concentration at 25°C. Adsorption isotherms were investigated by studying different temperatures (25°C, 35°C and 50°C) and initial NPX concentrations (20, 50, 100 and 150 mg/L). The NPX solution and the adsorbent prepared at the desired concentration were placed in a 50 mL centrifuge tube and 300 rpm stirring speed and adsorption experiments were performed at 25°C ± 1°C. After the adsorption process, the solutions were taken into falcon tubes and centrifuged at 3,000 rpm for 4 min. To determine the NPX concentration, the filtrate was taken with a syringe and analyzed in a UV spectrophotometer at a wavelength of 272 nm. Each experiment was repeated three times.

Maximum absorbance (λ_{max} = 272 nm) values were specified by scanning the absorbance values at different wavelengths (200–1,000 nm) of standard NPX solutions. Adsorption capacity and removal efficiency of NPX was calculated according to Eqs. (1) and (2), respectively.

$$q_e = \frac{\left(C_i - C_e\right)V}{m} \tag{1}$$

$$\text{Removal}\left(\%\right) = \frac{C_i - C_e}{C_i} \times 100 \tag{2}$$

where q_e (mg/g): adsorption capacity at equilibrium, V (L): volume of naproxen solution, m (g): amount of adsorbent, C_i (mg/L): initial concentration of NPX, C_e (mg/L): equilibrium concentration of NPX.

2.4. Desorption experiments and UV degradation

Desorption and regeneration are the most important aspects to establish the feasibility of the adsorption process. Water was used for the desorption of the NPX loaded GRO. Desorption efficiencies were calculated using Eq. (3).

$$\%\text{Desorption} = \frac{C_d \times V_d}{q_e \times W} \times 100 \tag{3}$$

where C_d (mg/L): desorbed adsorbate concentration, V_d (L): desorption solution volume, q_e (mg/g): amount of adsorbate pre-adsorbed to the adsorbent, W (g): mass of pre-adsorbed adsorbent.

UV degradation experiments were carried out on the ATLAS UV Test Device. Degradation processes were applied in UV Test Device ((Osram, 300 W) 1.55 W/m^2/nm irradiation, λ_{max} = 340 nm, high-pressure mercury UV lamp) at 60°C under UV light for different times (1–2–3 h).

2.5. Characterizations

NPX concentrations were measured using a UV spectrophotometer (Agilent Cary 60, USA). The solution pH was determined using HANNA HI 991001, USA model pH meter. Morphological appearance scanning electron microscopy (SEM-ZEISS Supra 40VP, USA), mineralogical content (HT-XRD; PANalytical Empyrean), functional group analysis Fourier-transform infrared spectroscopy (FT-IR; Perkin Elmer Spectrum 100, USA), surface areas (Brunauer–Emmett–Teller Theory – Micromeritics ASAP 2020) of adsorbents were determined.

3. Findings and discussion

3.1. Characterization of graphite oxide and graphite

When the structural properties of graphite and graphite oxide were examined, the outer surface area of GRO increased after oxidation, but the pore volume and width decreased (Table 1). In the study given in the literature, it was determined that graphite has a lower surface area but a higher pore volume [17].

X-ray diffraction (XRD) spectrum of graphite and graphite oxide is given in Fig. 2. In the graphite structure, the planes of graphene layers are observed in the form of very dense and narrow crests at 2θ = 26.5° [17]. The graphene peak at 2θ = 26.5° observed in the GRO structure was shorter than the peak observed in GR, because it may have been caused by the formation of residual oxygen functions between the graphene layers [27].

FT-IR spectra of graphite and graphite oxide structure are given in Fig. 3. While no significant peaks were observed in the graphite spectrum, the presence of

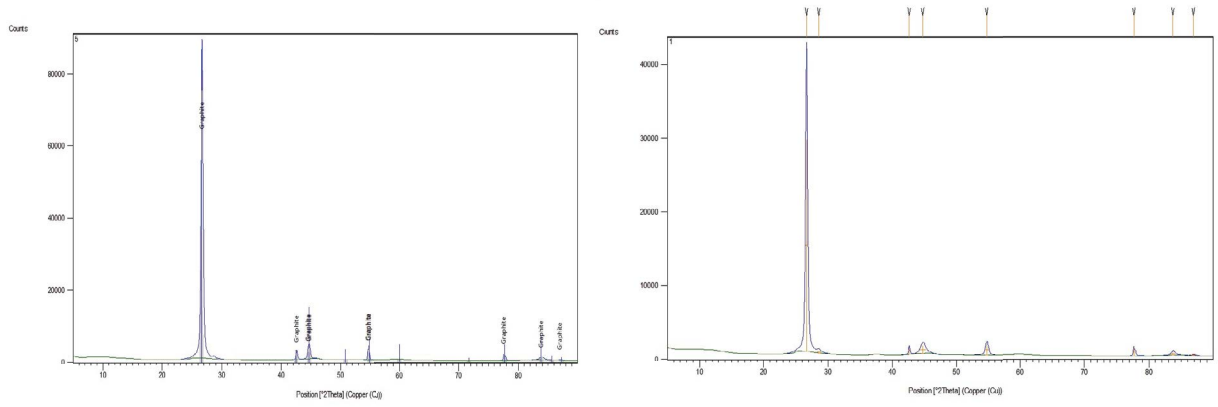

Fig. 2. XRD spectrum of graphite oxide and graphite (a) GR and (b) GRO.

various bands belonging to the oxygen-containing groups was observed in the graphite oxide spectrum. In the spectrum of GRO structure, the bands at wavenumbers 1,052; 1,385; 1,633; 2,916 and 3,446 cm^{-1}, were corresponded to stretching vibrations of C–O bonds [28], C–OH bending vibrations [29], stretching vibrations of O–H groups [30], $–CH_2$ stretching vibrations [31], bending vibrations of O–H groups [32], respectively. Observation of the graphite oxide structure characteristic peaks in the spectrum such as O–H stretch, C–OH bending and C–O stretch (alkoxy) showed that oxygen-based groups were effectively incorporated into the graphite structure and the oxidation process was successful [33].

Table 1
Surface area properties of graphite oxide and graphite

	GR	GRO
S_{BET} (m^2/g)	1.87	21.04
S_{ext} (m^2/g)	1.80	21.49
S_{mic} (m^2/g)	0.068	0
V_t (cm^3/g)	0.01	0.03
V_{mic} (cm^3/g)	0	0
V_{mezo} (cm^3/g)	0.01	0.03
Av. pore width (m^2/cm^3)	193.95	54.74
Pore size (Å)	32,020	2,851

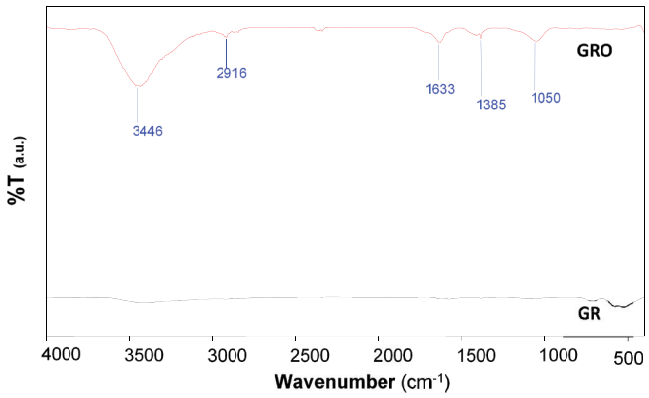

Fig. 3. FT-IR spectrum of graphite (GR) and graphite oxide (GRO).

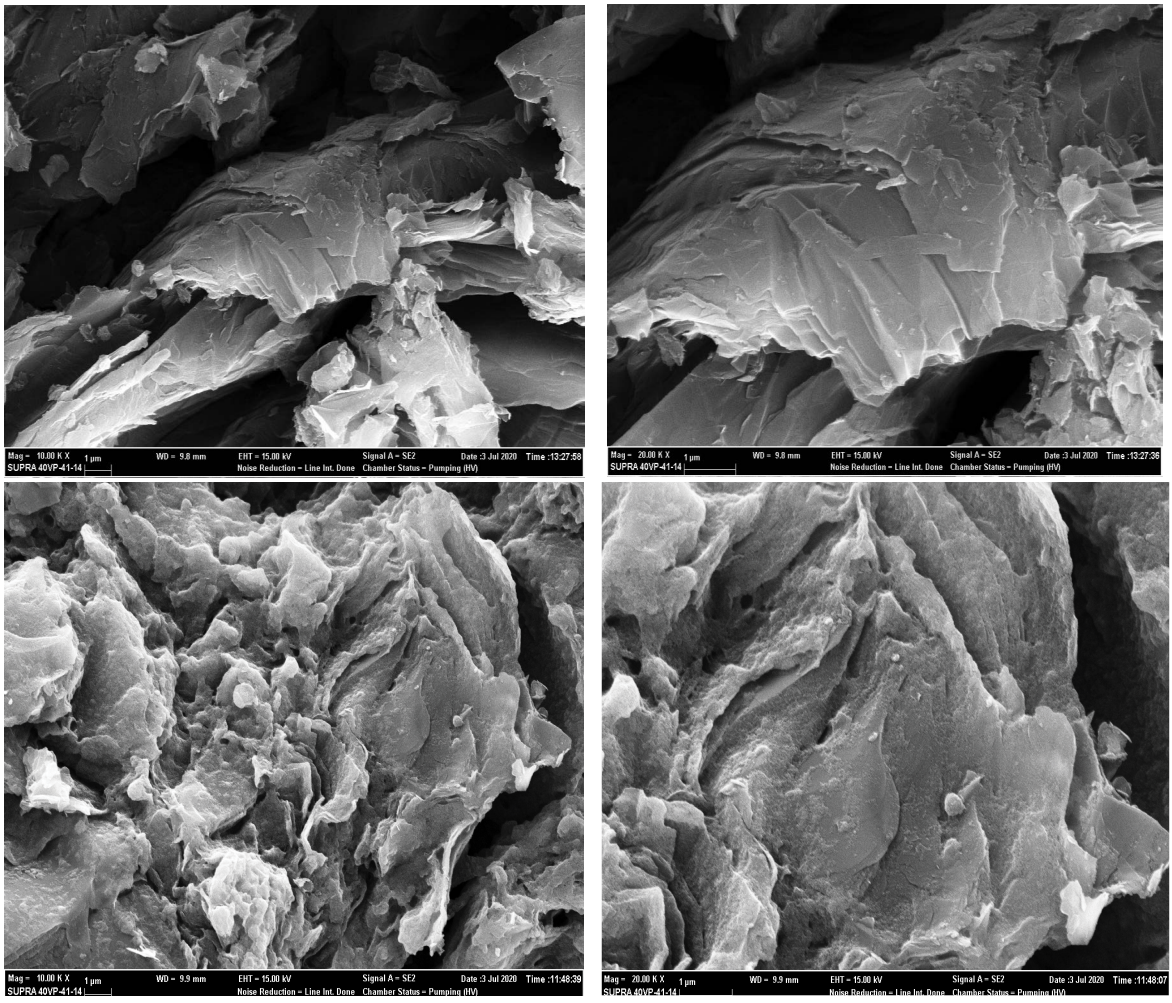

Fig. 4. SEM images of graphite and graphite oxide (left: 10,000X and right: 20,000X, top: GR and bottom: GRO).

In the SEM images of GR and GRO, it was observed that GR has a layered structure formed in layers. In the GRO structure, formations in the form of residues formed by functional structures after oxidation were observed (Fig. 4).

3.2. Adsorption behavior of NPX onto graphite oxide and graphite

GRO demonstrated fast adsorption kinetics for the adsorption of NPX, which reached dynamic equilibrium in a short time period (120 min) (Fig. 5a). The adsorption process activation energy was found to be much lower due to the effective Π–Π stacking interaction between GRO and NPX molecules, its excellent adsorption and good compatibility [34]. When the effect of pH on the removal efficiency of NPX was examined, the maximum removal efficiency was obtained for both GR and GRO at the natural pH of NPX (pH = 6) (Fig. 5b). NPX consists of hydrophilic and hydrophobic properties. Acidic and hydrophilic activity may occur due to hydrogen in the carboxylic group, which can be ionized (relative to its anionic form) at pH > pKa; hydrophobic properties were due to aliphatic rings [24]. NPX removal from aqueous solution remained approximately constant with varying amounts of GRO. Due to its hydrophilic properties, maximum removal efficiency of 67% was obtained for NPX using 3 g of GRO (Fig. 5c). It is clear that the adsorption of NPX onto GRO is highly dependent on the initial NPX concentration, and maximum removal efficiency for 150 ppm is 73% (at pH 6, GRO dose 3 g/50 mL, temperature 25°C ± 1°C and contact time 120 min) (Fig. 5d).

3.3. Adsorption dynamics

Lagergren's velocity equation describing pseudo-first-order is one of the most commonly used equations to explain adsorbate adsorption from liquid phase [35–37]. The pseudo-second-order kinetic model assumes that the solute adsorption rate is proportional to the regions on the adsorbent [37]. Mechanical aspects of adsorption such as chemical reaction, diffusion and mass transfer for NPX adsorption on GRO were determined by pseudo-first-order [Eq. (4)], pseudo-second-order [Eq. (5)] and intraparticle diffusion [Eq. (6)] methods.

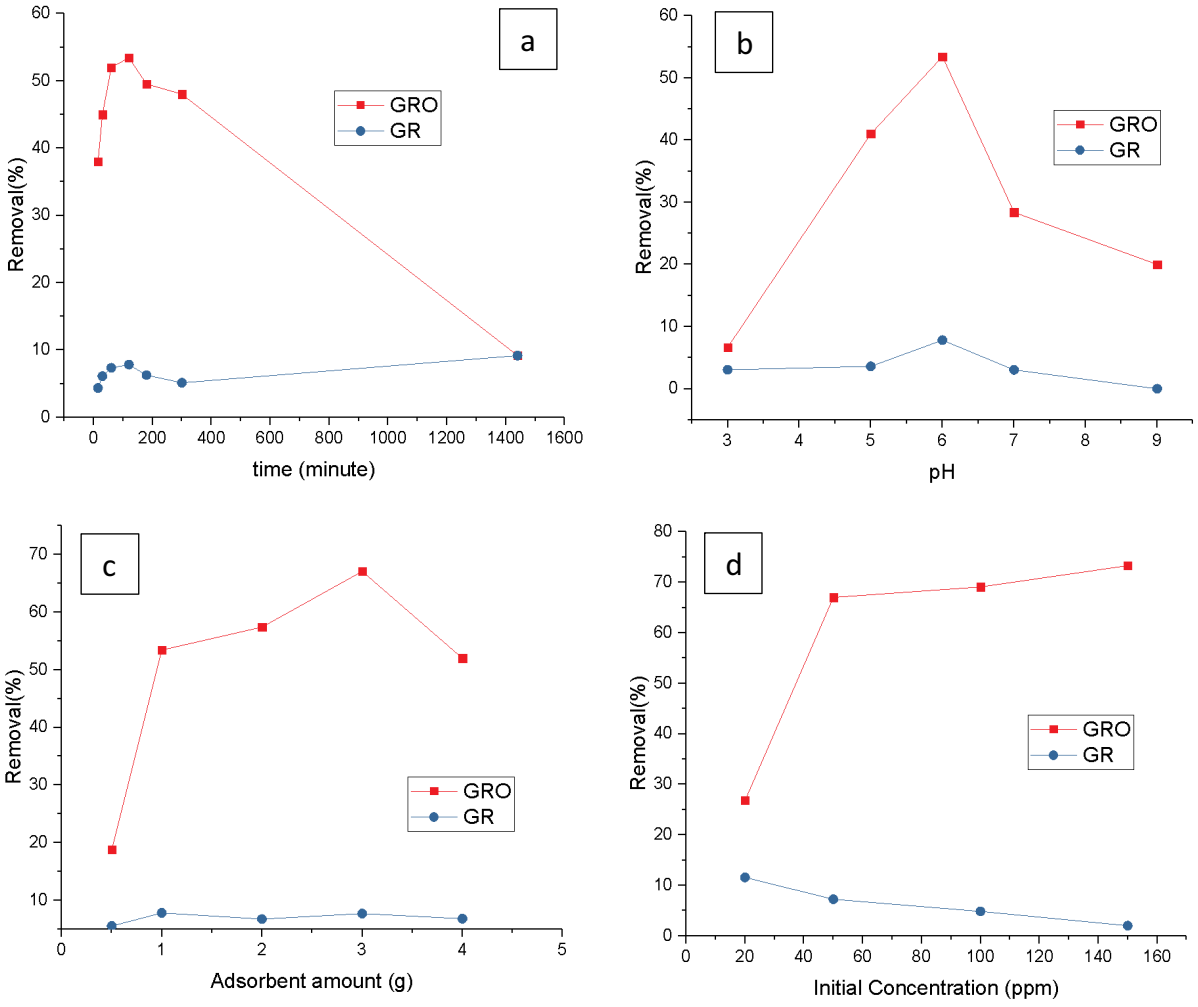

Fig. 5. Adsorption behavior of NPX onto graphite oxide and graphite: (a) contact time, (b) pH, (c) adsorbent amount, and (d) initial concentration (T = 25°C; mixing speed = 300 rpm; V = 50 mL)

$$\ln\left(q_e - q_t\right) = \ln q_e - k_1 t \tag{4}$$

$$\frac{t}{q_t} = \frac{1}{k_2 q_e^2} + \frac{t}{q_e} \tag{5}$$

$$q_e = K_i t^{0.5} + C \tag{6}$$

where q_t (mg/g) = adsorption capacity at t, q_e (mg/g) = adsorption capacity at equilibrium, k_1 and k_2; rate constants for pseudo-first-order model and pseudo-second-order model, t = time (min), K_i: velocity constant of intraparticle transport (g/mg min), C: constant.

Analysis results showed that the adsorption kinetics paired with the pseudo-second-order model (Fig. 6). Intraparticle diffusion did not occur due to low correlation values in all periods (Fig. 7).

3.4. Adsorption isotherm models

Nonlinear isotherm modeling has been used to determine the adsorption capacity and selectivity between adsorbates and adsorbents [38]. The adsorption isotherm shows how efficient the adsorption system is and how efficiently the adsorbate interacts with the adsorbent [39,40]. The isotherm analysis of the adsorption process was examined according to Langmuir, Freundlich and Temkin isotherm models. According to the Langmuir isotherm model, the adsorbent surface has a homogeneous structure and only one molecule can be adsorbed at each adsorption center. There is no interaction between the adsorbed molecules [41]. All adsorption areas on the adsorbent surface of an absorbent have a heterogeneous structure in the Freundlich isotherm model [42]. Temkin isotherm is generally used in systems where surface energy is heterogeneous (non-homogeneous distribution of adsorption heat) [43]. Langmuir isotherm [Eq. (7)], Freundlich isotherm [Eq. (8)], The Temkin isotherm [Eq. (9)] models are given below.

$$\frac{C_e}{q_e} = \frac{C_e}{q_{\max}} + \frac{1}{K_L q_{\max}} \tag{7}$$

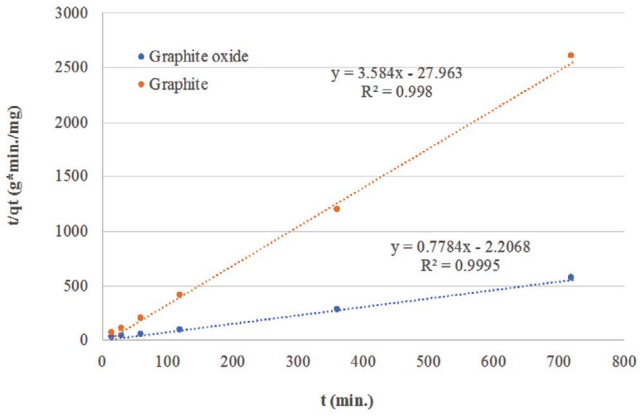

Fig. 6. Second stage model kinetics on GRO and GR of NPX adsorption.

$$\ln q_e = \ln K_f + \frac{\ln C_e}{n} \tag{8}$$

$$q_e = \frac{RT}{b}\ln A + \frac{RT}{b}\ln C_e \tag{9}$$

where q_e: amount of NPX for each mass of adsorbent (mg/g), C_e: concentration at equilibrium (mg/L), $q_{\max}$: maximum NPX adsorption capacity as theoretical (mg/g), K_L: Langmuir constant (L/mg), K_f, n: Freundlich constants, A (slope): binding constant in equilibrium of Temkin isotherm (L/g), b (intercept): Temkin isotherm constant, R: general gas constant (8.314 J/mol K), T: temperature (K).

Langmuir, Freundlich and Temkin isotherm correlation coefficients of NPX on the adsorbents are given in Table 2. It was determined that the adsorption of NPX on GRO fitted all three models (Langmuir, Freundlich and Temkin isotherm models). Freundlich R^2 = 1.00 > Langmuir R^2 = 0.99 = Temkin R^2 = 0.99. It was determined that the adsorption of NPX on GR fitted the best Temkin isotherm model. Temkin R^2 = 0.99 > Langmuir R^2 = 0.93 > Freundlich R^2 = 0.87 (Figs. 8–10).

There is no study in the literature about the removal of NPX by adsorption using graphite oxide. However, the closest study to our study was conducted by Ciğeroğlu et al. [21]. They adsorbed NPX on graphene oxide. It was determined that the graphene oxide surface has a multilayer heterogeneous system structure according to Freundlich (R^2 > 0.90) and Halsey (R^2 > 0.93) isotherms. In our study, it was determined that the adsorbent surface is both homogeneous and heterogeneous since the adsorption of

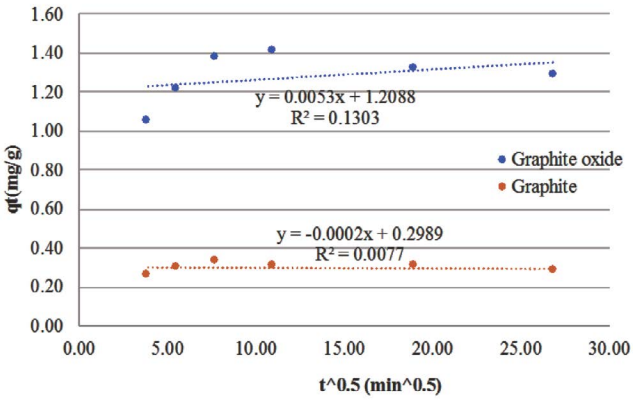

Fig. 7. Intraparticle diffusion model on GRO and GR of NPX adsorption.

Table 2
Langmuir, Freundlich and Temkin isotherms correlation coefficients of NPX adsorption on adsorbents

	R^2		
	Langmuir	Freundlich	Temkin
GR	0.93	0.87	0.99
GRO	0.99	1.00	0.99

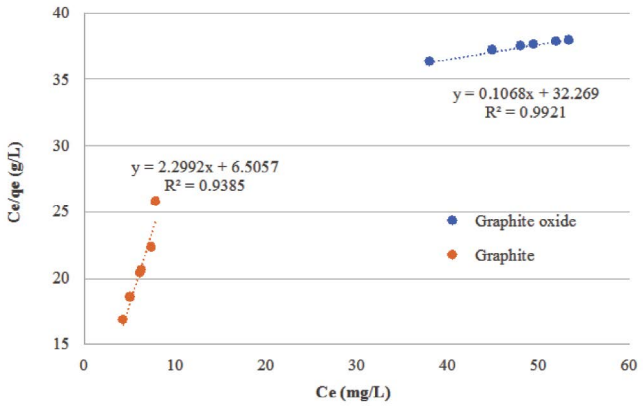

Fig. 8. Langmuir isotherm model.

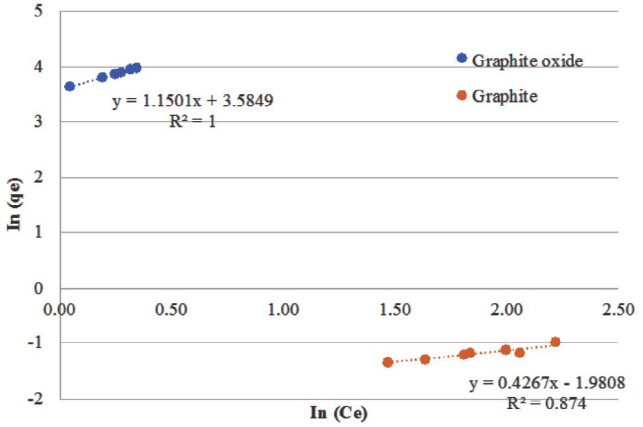

Fig. 9. Freundlich isotherm model.

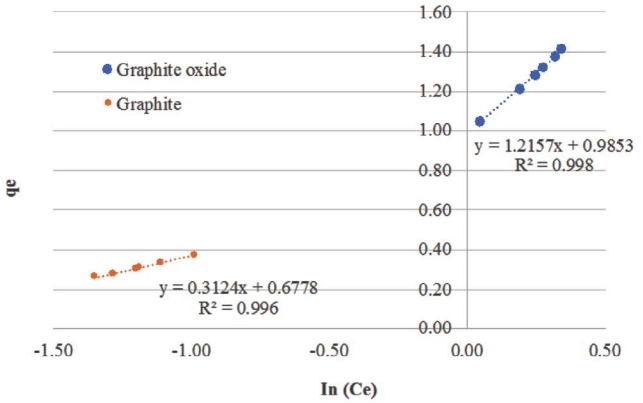

Fig. 10. Temkin isotherm model.

NPX on graphite oxide conforms to Freundlich (R^2 = 1.00), Langmuir (R^2 = 0.99) and Temkin (R^2 = 0.99) isotherms.

3.5. Thermodynamic parameters

When the adsorption capacity of GR and GRO's NPX was examined, the adsorption capacity of GR and GRO's NPX decreased as the temperature increased (Fig. 11).

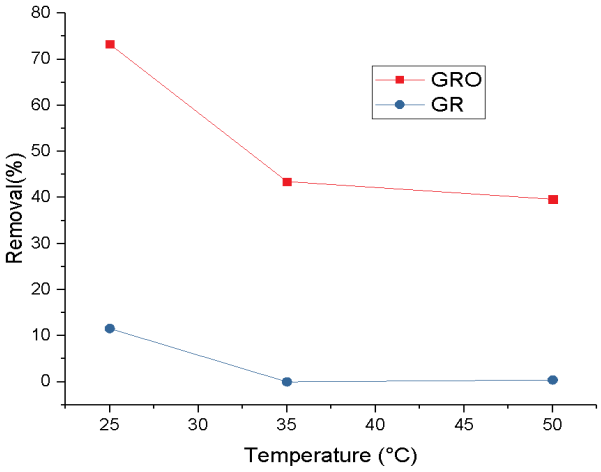

Fig. 11. Temperature effect on adsorption behavior of NPX onto GRO and GR.

Different useful parameters calculated using Van't Hoff charts are evaluated to give an idea of the thermodynamic aspects of the adsorption process. The Gibbs free energy difference ($\Delta G°$) of the adsorption process is related to the equilibrium constant of the Van't Hoff equation [Eq. (10)]. The Gibbs free energy difference ($\Delta G°$) is associated with entropy change at constant temperature ($\Delta S°$) and adsorption temperature ($\Delta H°$) as regards to thermodynamics [Eq. (11)].

$$\Delta G° = -RT \ln K_d \tag{10}$$

$$\ln K_d = \frac{\Delta S°}{R} - \frac{\Delta H°}{RT} \tag{11}$$

where T: temperature (K), R: ideal gas constant (8.314 J/mol K). $\Delta S°$ and $\Delta H°$ were calculated by plotting $1/T$ against $\ln K_d$ with the help of Van't Hoff curve. For the GRO adsorbent, $\Delta H°$ (kJ/mol), $\Delta S°$ (kJ/mol) and $\Delta G°$ (kJ/mol) values were calculated as –3,119.3, 6.7059 and –10,028.1, respectively (Fig. 12). These calculations could not be made for the GR due to the loss of the adsorption capacity of the GR due to the increase in temperature (Fig. 12). The negative $\Delta H°$ value for the GRO adsorbent indicated that the adsorption process was exothermic, during the adsorption of the solid/solution interface, the positive $\Delta S°$ value increased randomly, the negative $\Delta G°$ value showed that the adsorption process occurred spontaneously.

FT-IR spectra of graphite oxide and naproxen adsorbed graphite oxide (NPX-GRO) structures are shown in Fig. 13. It was observed that in the spectrum of the NPX-GRO structure, the peaks at wavenumbers 1,029; 1,230; 1,249; 1,395 and 1,480 cm^{-1} were attributed to aryl-O asymmetric stretching vibrations, –O–stretching vibrations, aryl-O symmetric stretching vibrations, CH_3 bonds bending vibrations [44] and C=C aromatic stress vibrations [45], respectively. The occurrence of these peaks in the spectrum, which is specific for the NPX structure, showed that naproxen was adsorbed on the GRO structure. The observation that the vibrations of C–O bonds have seen

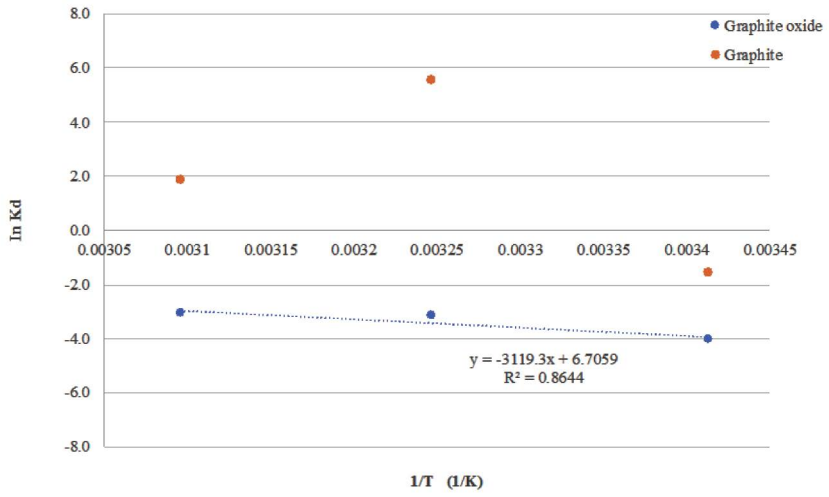

Fig. 12. $\ln K_d - 1/T$ graph.

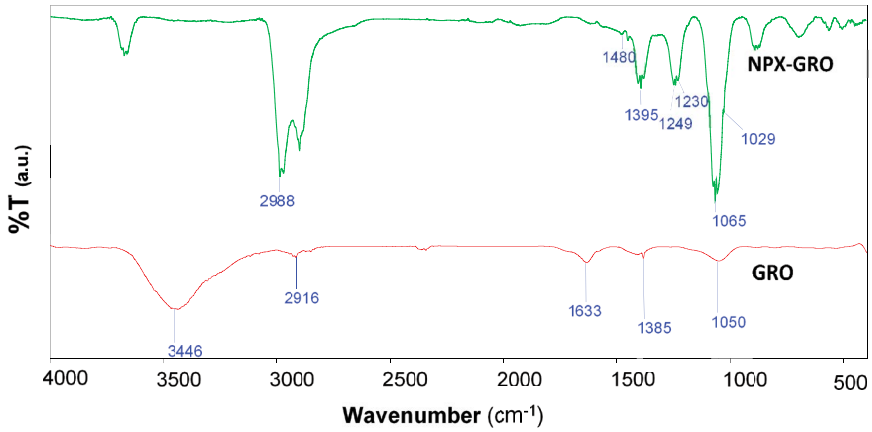

Fig. 13. FT-IR spectrum of graphite oxide (GRO) and naproxen adsorbed graphite oxide (NPX-GRO).

at 1,050 cm^{-1} in the spectrum of the GRO structure shifted to 1,065 cm^{-1} after naproxen adsorption, was interpreted as the adsorption of NPX. In addition, the significant increase in peak intensity was attributed to the presence of C–O bonds in the NPX structure. The shift in the C–O band is likely due to the NPX interacting with the C–O.

3.6. UV degradation effect on NPX adsorbed GRO

Carbonaceous species not only stimulate light-sensitive visible light absorption and response, but also increase photoquantum efficiency [46]. In the study where activated carbons were used as catalysts, a good photodegradation efficiency was obtained for organic pollutants in the absence of semiconductor additives. It was observed that interactions occur between carbon particles and UV light [47]. It was observed that naproxen undergoes direct photodegradation within hours by absorbing UV light up to 360 nm in an aqueous environment [48].

The optimum adsorption conditions of NPX were explained; 3 g/50 mL adsorbent amount, 150 ppm initial concentration, pH 6, for 120 min at 25°C for GRO and 3 g/50 mL adsorbent amount, 20 ppm initial concentration, pH 6, for 120 min at 25°C for GR.

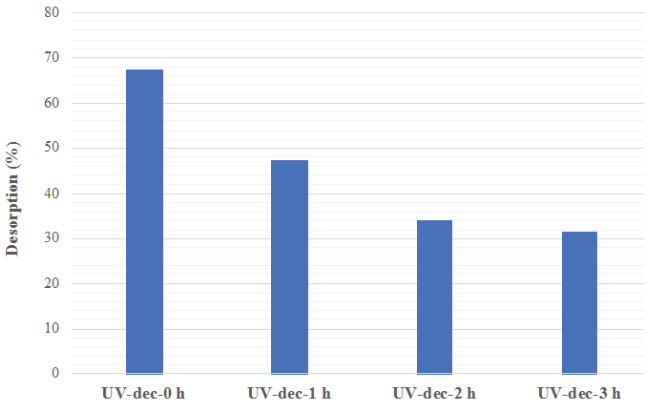

Fig. 14. Desorption studies of UV degradation.

In order to determine the UV degradation of NPX adsorbed by GRO, the UV degradation effect of adsorbed GRO desorbed in water was investigated. Maximum

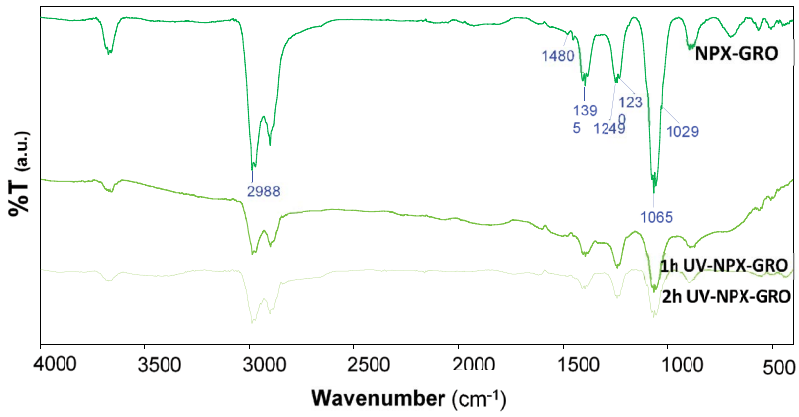

Fig. 15. FT-IR spectrum of naproxen adsorbed graphite oxide (NPX-GRO) and UV degraded naproxen adsorbed graphite oxide (1 and 2 h).

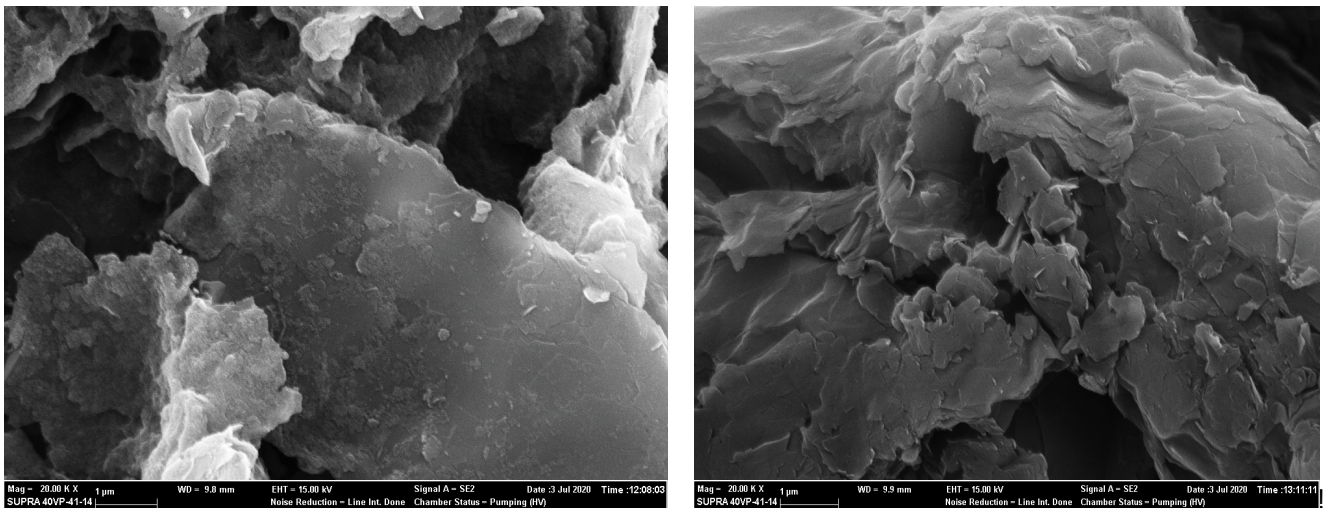

Fig. 16. SEM images of adsorbed GRO (a) and GRO (b) after 2 h of UV degradation (20,000X).

adsorption removal efficiency at optimum conditions determined for each adsorbent was 11.56% for GR and 73.29% for GRO. Since the removal efficiency of GR was very low, UV degradation studies of NPX were applied only for GRO. 67.5% of the NPX adsorbed on GRO at 1 h was desorbed into water. The determination of the desorption % of adsorbed GRO as 47.5%, 34.06% and 31.59% at the end of 1 h, 2 h and 3 h in UV degradation studies, respectively proved that UV degradation was effective in removing the adsorbed NPX on the GRO surface (Fig. 14). This has shown that in the anhydrous and semiconductor-free environment, carbon-photon interactions occur that can spread across the GRO layers and reach molecules adsorbed in porosity.

3.6.1. FT-IR analysis

Removal of naproxen adsorbed on GRO was investigated by UV degradation for 1 and 2 h (Fig. 15). According to FT-IR analysis, the observation of a significant decrease in the intensity of all peaks (especially, specific peaks of naproxen; 1,230; 1,249; 1,395; 1,480 and 1,065 cm^{-1}) after UV degradation showed that NPX adsorbed to GRO could be removed under the effect of UV. In addition, it was observed that the spectra obtained after the degradation process for 1 and 2 h were quite similar.

3.6.2. SEM images

The SEM images obtained at the end of 1 and 2 h of UV degradation studies of adsorbed GRO's are given in Fig. 16. After 2 h of UV degradation, it was observed that the residues formed by functional structures on the GRO surface (structures formed after both oxidation and adsorption) were removed.

4. Conclusions

The removal of naproxen adsorbed on graphite oxide produced from commercial graphite by degradation under UV effect was investigated in this study. The optimum adsorption conditions of GR and GRO adsorbents used in the adsorption of NPX were explained; pH 6, 3 g/50 mL adsorbent amount at 25°C, 150 ppm initial concentration, 120 min contact time for GRO and pH 6, 3 g/50 mL

adsorbent amount at 25°C, 20 ppm initial concentration, 120 min contact time for GR. Maximum removal efficiencies at optimum conditions determined for each adsorbent were 11.56% for GR and 73.29% for GRO.

Since the removal efficiency of GR was very low, UV degradation studies of NPX have been applied only for GRO. 67.5% of the NPX adsorbed on GRO was desorbed into water. The determination of the desorption % of adsorbed GRO as 47.5%, 34.06% and 31.59%, respectively, at the end of 1, 2 and 3 h in UV degradation studies, proved that UV degradation was effective in removing the adsorbed NPX on the GRO surface. As a result, it was observed that UV degradation was effective in removing NPX from the GRO surface.

Acknowledgments

Thank you to SKC Carbon San. ve Tic. A.Ş. for its graphite sample support. The authors would like to acknowledge the authors' student Cemal Tugrul Bilgic for their kind help and assistance. There is no conflict of interest between the parties.

References

[1] E. Nyankson, R.V. Kumar, Removal of water-soluble dyes and pharmaceutical wastes by combining the photocatalytic properties of Ag_3PO_4 with the adsorption properties of halloysite nanotubes, Mater. Today Adv., 4 (2019) 100025, doi: 10.1016/j.mtadv.2019.100025.

[2] J. Lach, A. Szymonik, Adsorption of naproxen sodium from aqueous solutions on commercial activated carbons, J. Ecol. Eng., 20 (2019) 241–251.

[3] M. Qurie, M. Khamis, F. Malek, S. Nir, S.A. Bufo, J. Abbadi, L. Scrano, R. Karaman, Stability and removal of naproxen and its metabolite by advanced membrane wastewater treatment plant and micelle-clay complex, Clean – Soil Air Water, 42 (2014) 594–600.

[4] G.R. Boyd, S. Zhang, D.A. Grimm, Naproxen removal from water by chlorination and biofilm processes, Water Res., 39 (2005) 668–676.

[5] D. Górny, U. Guzik, K. Hupert-Kocurek, D. Wojcieszyńska, Naproxen ecotoxicity and biodegradation by *Bacillus thuringiensis* B1(2015b) strain, Ecotoxicol. Environ. Saf., 167 (2019) 505–512.

[6] T. Ding, K. Lin, B. Yang, M. Yang, J. Li, W. Li, J. Gan, Biodegradation of naproxen by freshwater algae *Cymbella* sp. and *Scenedesmus quadricauda* and the comparative toxicity, Bioresour. Technol., 238 (2017) 164–173.

[7] Q. Li, P. Wang, L. Chen, H. Gao, L. Wu, Acute toxicity and histopathological effects of naproxen in zebrafish (*Danio rerio*) early life stages, Environ. Sci. Pollut. Res., 23 (2016) 18832–18841.

[8] M.H. Ahmad, M. Fatima, M. Hossain, A.C. Mondal, Evaluation of naproxen-induced oxidative stress, hepatotoxicity and in-vivo genotoxicity in male Wistar rats, J. Pharm. Anal., 8 (2018) 400–406.

[9] F.J. Benitez, J. Acero, F. Real, G. Roldán, E. Rodriguez, Ultrafiltration and nanofiltration membranes applied to the removal of the pharmaceuticals amoxicillin, naproxen, metoprolol and phenacetin from water, J. Chem. Technol. Biotechnol., 86 (2011) 858–866.

[10] K.A. Landry, P.Z. Sun, C.-H. Huang, T.H. Boyer, Ion-exchange selectivity of diclofenac, ibuprofen, ketoprofen, and naproxen in ureolyzed human urine, Water Res., 68 (2015) 510–521.

[11] R. Mailler, J. Gasperi, G. Chebbo, V. Rocher, Priority and emerging pollutants in sewage sludge and fate during sludge treatment, Waste Manage., 34 (2014) 1217–1226.

[12] L. Rizzo, Bioassays as a tool for evaluating advanced oxidation processes in water and wastewater treatment, Water Res., 45 (2011) 4311–4340.

[13] F.J. Beltrán, P. Pocostales, P. Alvarez, A. Oropesa, Diclofenac removal from water with ozone and activated carbon, J. Hazard. Mater., 163 (2009) 768–776.

[14] J.L. Gong, Y.L. Zhang, Y. Jiang, G.M. Zeng, Z.H. Cui, K. Liu, C.H. Deng, Q.Y. Niu, J.H. Deng, S.Y. Huan, Continuous adsorption of Pb(II) and methylene blue by engineered graphite oxide coated sand in fixed-bed column, Appl. Surf. Sci., 330 (2015) 148–157.

[15] G. Ghanashyam, H.K. Jeong, Synthesis of plasma treated nitrogen-doped graphite oxide for supercapacitor applications, J. Energy Storage, 26 (2019) 100923, doi: 10.1016/j.est.2019.100923.

[16] X. Lei, X. Li, Z. Ruan, T. Zhang, F. Pan, Q. Li, D. Xia, J. Fu, Adsorption-photocatalytic degradation of dye pollutant in water by graphite oxide grafted titanate nanotubes, J. Mol. Liq., 266 (2018) 122–131.

[17] T. Hartono, S. Wang, Q. Ma, Z. Zhu, Layer structured graphite oxide as a novel adsorbent for humic acid removal from aqueous solution, J. Colloid Interface Sci., 333 (2009) 114–119.

[18] F.B. Bujans, S. Cerveny, R. Verdejo, J.J. del Val, J.M. Alberdi, A. Alegría, J. Colmenero, Permanent adsorption of organic solvents in graphite oxide and its effect on the thermal exfoliation, Carbon, 48 (2010) 1079–1087.

[19] M. Lojka, B. Lochman, O. Jankovský, A. Jiříčková, Z. Sofer, D. Sedmidubský, Synthesis, composition, and properties of partially oxidized graphite oxides, Materials (Basel)., 12 (2019) 2367, doi: 10.3390/ma12152367.

[20] R. Muzyka, M. Kwoka, Ł. Smędowski, N. Díez, G. Gryglewicz, Oxidation of graphite by different modified Hummers methods, Xinxing Tan Cailiao/New Carbon Mater., 32 (2017) 15–20.

[21] Z. Ciğeroğlu, O.K. Özdemir, S. Şahin, A. Haşimoğlu, Naproxen adsorption onto graphene oxide nanopowders: equilibrium, kinetic, and thermodynamic studies, Water Air Soil Pollut., 231 (2020) 1–10.

[22] N.N. Naing, S.F.Y. Li, H.K. Lee, Graphene oxide-based dispersive solid-phase extraction combined with in situ derivatization and gas chromatography-mass spectrometry for the determination of acidic pharmaceuticals in water, J. Chromatogr. A, 1426 (2015) 69–76.

[23] M. Sarker, J.Y. Song, S.H. Jhung, Adsorptive removal of anti-inflammatory drugs from water using graphene oxide/metal-organic framework composites, Chem. Eng. J., 335 (2018) 74–81.

[24] O. Paunovic, S. Pap, S. Maletic, M.A. Taggart, N. Boskovic, M.T. Sekulic, Ionisable emerging pharmaceutical adsorption onto microwave functionalised biochar derived from novel lignocellulosic waste biomass, J. Colloid Interface Sci., 547 (2019) 350–360.

[25] A.E. Neal, P.A. Moore, Mimicking natural systems: changes in behavior as a result of dynamic exposure to naproxen, Ecotoxicol. Environ. Saf., 135 (2017) 347–357.

[26] M. Yazıcı, İ. Tiyek, M.S. Ersoy, M.H. Alma, U. Dönmez, B. Yıldırım, T. Salan, Ş. Karataş, S. Uruş, İ. Karteri, K. Yıldız, Modifiye Hummers Yöntemiyle Grafen Oksit (GO) Sentezi ve Karakterizasyonu, Gazi Univ. J.l of Sci. GU J Sci Part C, 4 (2016) 41–48.

[27] R.K. Siddarth, M. Manopriya, G. Swathi, G. Vijayvenkataraman, K.R. Aranganayagam, One Step Synthesis of Reduced and *Moringa oleifera* Treated Graphene Oxide: Characterization and Antibacterial Studies, M. Rajan, K. Anand, A. Chuturgoon, Eds., Proceedings of the International Conference on Nanomedicine (ICON-2019), Springer Proceedings in Materials, Springer, Cham, 2019, pp. 54–62.

[28] K. Zhou, Y. Zhu, X. Yang, X. Jiang, C. Li, Preparation of graphene-TiO_2 composites with enhanced photocatalytic activity, New J. Chem., 35 (2011) 353–359.

[29] B. Kartick, S.K. Srivastava, I. Srivastava, Green synthesis of graphene, J. Nanosci. Nanotechnol., 13 (2013) 4320–4324.

[30] L. Pan, J.J. Zou, S. Wang, X.Y. Liu, X. Zhang, L. Wang, Morphology evolution of TiO_2 facets and vital influences on photocatalytic activity, ACS Appl. Mater. Interfaces, 4 (2012) 1650–1655.

[31] W.S. Wang, D.H. Wang, W.G. Qu, L.Q. Lu, A.W. Xu, Large ultrathin anatase TiO_2 nanosheets with exposed {001} facets on graphene for enhanced visible light photocatalytic activity, J. Phys. Chem. C, 116 (2012) 19893–19901.
[32] M.S.A.S. Shah, A.R. Park, K. Zhang, J.H. Park, P.J. Yoo, Green synthesis of biphasic TiO_2–reduced graphene oxide nanocomposites with highly enhanced photocatalytic activity, ACS Appl. Mater. Interfaces, 4 (2012) 3893–3901.
[33] N. Pan, D. Guan, T. He, R. Wang, I. Wyman, Y. Jin, C. Xia, Removal of Th^{4+} ions from aqueous solutions by graphene oxide, J. Radioanal. Nucl. Chem., 298 (2013) 1999–2008.
[34] G. Zhao, J. Li, X. Wang, Kinetic and thermodynamic study of 1-naphthol adsorption from aqueous solution to sulfonated graphene nanosheets, Chem. Eng. J., 173 (2011) 185–190.
[35] S.K. Lagergren, About the theory of so-called adsorption of soluble substances, Sven. Vetenskapsakad. Handingarl., 24 (1898) 1–39.
[36] J. Weber Jr., W.J. Morris, J.C. Sanit, Kinetics of adsorption on carbon from solution, J. Sanit. Eng. Div., 89 (1963) 31–38.
[37] Y.S. Ho, G. McKay, Pseudo-second-order model for sorption processes, Process Biochem., 34 (1999) 451–465.
[38] A. Solanki, T.H. Boyer, Physical-chemical interactions between pharmaceuticals and biochar in synthetic and real urine, Chemosphere, 218 (2019) 818–826.
[39] S. Debnath, N. Ballav, A. Maity, K. Pillay, Competitive adsorption of ternary dye mixture using pine cone powder modified with β-cyclodextrin, J. Mol. Liq., 225 (2017) 679–688.
[40] B.S. Chittoo, C. Sutherland, Adsorption of phosphorus using water treatment sludge, J. Appl. Sci., 14 (2014) 3455–3463.
[41] I. Langmuir, The adsorption of gases on plane surfaces of glass, mica and platinum, J. Am. Chem. Soc., 40 (1918) 1361–1403.
[42] H. Freundlich, Über die Adsorption in Lösungen, Zeitschrift Für Phys. Chemie., 57U (2017) 385–470.
[43] M. Erhayem, F. Al-Tohami, R. Mohamed, K. Ahmida, Isotherm, kinetic and thermodynamic studies for the sorption of mercury(II) onto activated carbon from leaves, Am. J. Anal. Chem., 6 (2015) 1–10.
[44] M.F. Canbolat, A. Celebioglu, T. Uyar, Drug delivery system based on cyclodextrin-naproxen inclusion complex incorporated in electrospun polycaprolactone nanofibers, Colloids Surf., B, 115 (2014) 15–21.
[45] J. Akbari, M. Saeedi, K.M. Semnani, S. Sohrab, R. Masoumeh, A. Kofi, A.A.A. Nokhodchi, S.S. Rostamkalaei, M. Asadi, K.A. Addo, A. Nokhodchi, The design of naproxen solid lipid nanoparticles to target skin layers, Colloids Surf., B, 145 (2016) 626–633.
[46] Z. Yan, W. Gong, Y. Chen, D. Duan, J. Li, W. Wang, J. Wang, Visible-light degradation of dyes and phenols over mesoporous titania prepared by using anthocyanin from red radish as template, Int. J. Photoenergy, 2014 (2014) 968298, doi: 10.1155/2014/968298.
[47] L.F. Velasco, I.M. Fonseca, J.B. Parra, J.C. Lima, C.O. Ania, Photochemical behaviour of activated carbons under UV irradiation, Carbon, 50 (2012) 249–258.
[48] C. Cory, W. Desantis, C.Z. Ulmer, Photodegradation of Naproxen and Ibuprofen and the Formation of Ecotoxic Photoproducts in Natural Water Systems, IWA Specialty Conference on Natural Organic Matter, Costa Mesa, CA, USA, 2011.